

Ultrafast laser-induced magneto-optical changes in resonant magnetic x-ray reflectivity

Ivar Kumberg ¹, Evangelos Golias ¹, Sebastien E. Hadjadj ¹, Rahil Hosseinifar ¹, Sangeeta Thakur ¹, Tauqir Shinwari ¹,
 Ismet Gelen ¹, Niko Pontius ², Christian Schüßler-Langeheine ², Clemens von Korff Schmising ³,
 Sangeeta Sharma ³ and Wolfgang Kuch ^{1,*}

¹*Institut für Experimentalphysik, Freie Universität Berlin, Arnimallee 14, 14195 Berlin, Germany*

²*Helmholtz-Zentrum Berlin für Materialien und Energie, Albert-Einstein-Straße 15, 12489 Berlin, Germany*

³*Max-Born-Institut für Nichtlineare Optik und Kurzzeitspektroskopie, Max-Born-Straße 2A, 12489 Berlin, Germany*



(Received 3 April 2023; accepted 7 August 2023; published 28 August 2023)

We investigate the magneto-optical response of Co to an ultrashort laser excitation by x-ray resonant magnetic reflectivity (XRMR) employing circular polarization. The time-resolved reflectivities detected for opposite sample magnetization are separated into magnetic and nonmagnetic contributions, which contain information about the structural, electronic, and magnetic properties of the sample. Different response times of the different contributions are observed. The experimental results are reproduced numerically by two different simulation approaches. On the one hand, we use a purely thermal model, a time-dependent heat-induced loss of macroscopic magnetization, and an inhomogeneous laser-induced strain profile. On the other hand, we employ time-dependent density-functional theory to calculate the transient optical response to the laser-induced excitation and from that the reflected intensities. While both methods are able to reproduce the time dependence of the magnetic signal, the ultrafast nonmagnetic change in reflectivity is captured satisfactorily only in simulations of the transient optical response function and has thus to be assigned to electronic effects. The energy dependence of the magnetic circular dichroism is investigated in the simulations, highlighting a dependence of the observable on the probing energy. Finally, a phenomenological explanation of the dynamics measured in dichroic x-ray reflectivity in the different channels is offered.

DOI: [10.1103/PhysRevB.108.054439](https://doi.org/10.1103/PhysRevB.108.054439)

I. INTRODUCTION

Experimental studies of ultrafast demagnetization processes, initiated by the first experimental investigation of the ultrafast demagnetization of Ni using time-resolved magneto-optical Kerr effect by Beaurepaire *et al.* [1], have developed into an own field of research (see Refs. [2–5] and references therein). Such studies are essential for the understanding of ultrafast magnetization dynamics and have led to substantial insight into the underlying physical mechanisms and their theoretical description, such as, for example, the microscopic three-temperature model [6]. Combining ultrashort soft-x-ray probe pulses with near-infrared pump pulses to follow the magnetic response of an excited system [7–16] contributes an invaluable method to this field to meet the high demands of time- and element-resolved studies of ultrafast magnetism. It is particularly the elemental resolution of this approach that has helped to identify the role of the different timescales of demagnetization of $3d$ and $4f$ elements in ferrimagnetic alloys for the ultrafast laser-induced all-optical magnetic switching [10], prove the presence of nonlocal spin transport in ultrafast demagnetization [11], and has led to a number of investigations disentangling the complex evolution of the magnetic

system, spin and electron scattering, as well as transport upon intense optical excitation [10,11,13,16].

Soft-x-ray resonant magnetic reflectivity (XRMR) is a powerful method for the investigation of magnetic properties of thin films and surfaces that can provide at the same time information about the structure and morphology of the sample as well as magnetization depth profiles [17–21] and has already been also used successfully for the study of ultrafast demagnetization by magnetic circular dichroism [22–25]. For the study of ultrafast processes in samples on crystalline substrates or with buried layers, it typically provides much higher signals than total-electron-yield detection of x-ray absorption, which is important considering the often very low average fluence of sources of pulsed x rays. In such dichroic measurements, typically the difference of the recorded intensities for opposite helicity or magnetization are considered as magnetic signal, while the independent channels are usually not studied in detail.

In absorption experiments that probe the full range of the electronic transitions, e.g., the entire $L_{2,3}$ edge in $3d$ ferromagnets (FMs), the orbital and effective spin magnetic moments are indeed directly linked to the magnetic circular dichroism signal by sum rules [26]. However, in time-resolved studies, the magnetization of the system is usually probed as a function of time at only one specific electronic excitation, i.e., at limited energy bandwidth, because of the small figure of merit of these experiments. For x-ray absorption experiments, the effect of the transient repopulation of electronic states due to

*Correspondence and requests for materials should be addressed: kuch@physik.fu-berlin.de

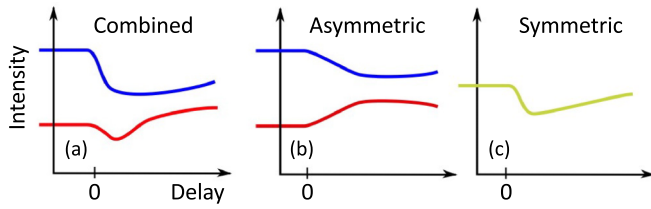


FIG. 1. Sketch of the acquired signals in a resonant soft x-ray pump-probe dichroism experiment. (a) In the experiment, two time traces are obtained, one for each circular helicity or direction of sample magnetization ($M+$ and $M-$). The intensity recorded resonantly changes over delay time after the excitation of the sample due to a reduction of the magnetic dichroism (b) and due to a change of the helicity-averaged reflectivity (c). The combined signal measured in the experiment is described by the sum of both.

the excitation has already been discussed and has to be kept in mind when interpreting the time evolution of the signal in terms of the evolution of the temporal magnetic state of the system [27,28].

Here, we extend this discussion to time-resolved XRMR. In XRMR, where the specularly reflected x-ray intensity is measured instead of the x-ray absorption, a further complication arises due to the influence of transient changes of the refractive properties of the sample, i.e., the real part of the refractive index, in contrast to absorption experiments, which probe only the imaginary part. We take a closer look into the separate channels recorded in a time-resolved XRMR measurement of the ultrafast demagnetization of Co as a model system. Circularly polarized x rays are employed to be sensitive to the sample magnetization. The helicity-dependent excitation probabilities of the $2p-3d$ transitions give rise to a difference in the absorption of circularly polarized x rays in the presence of magnetization. The intensity of the specularly reflected x rays under a certain angle is recorded, which contains information about the magnetic properties, structure, sample geometry, and electronic population. Figure 1 illustrates the dynamics of the two individual channels recorded in a time-resolved experiment. The measured signal [Fig. 1(a)] can be sketched as a combination of an antisymmetric and a symmetric response of the two channels to an ultrafast laser pulse, reflected by the difference and the sum of the two channels, respectively. The antisymmetric response, i.e., the helicity dependence of the reflectivity, thereby has to be of magnetic origin. We will elucidate in the following how the transient magnetic and nonmagnetic changes of the sample affect the measured signals.

In order to identify the different contributions to the transient change in x-ray reflectivity, we compare experimental data to two different theoretical simulations. In one case, we model the response of the sample by a time-dependent macroscopic magnetization and a time-dependent strain profile across the sample. In the other case, time-dependent density-functional theory (TD-DFT) is employed to calculate the response of the electronic system of the sample and from that the time-dependent complex refractive index. Since only the latter can reproduce the experimentally observed ultrafast nonmagnetic change of the reflected intensity, we conclude that it is mainly due to electronic excitations. We compare our

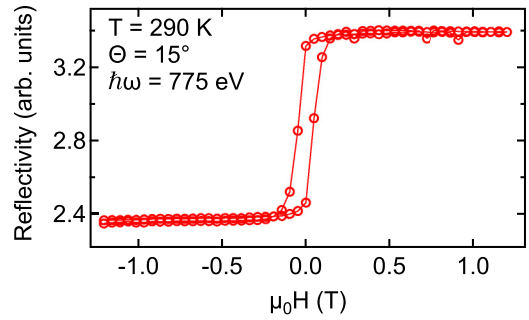


FIG. 2. Hysteresis loop of the sample at 290 K, measured *in situ* in reflectivity at 15° between surface and incident beam and 775 eV photon energy.

results to previous time-resolved investigations of Co films on Cu(001), which were carried out by methods without elemental resolution [29–32].

II. EXPERIMENT

The investigation is performed on a 61 monolayer (ML) Cu/15 ML Co/20 ML $\text{Ni}_{31}\text{Mn}_{69}$ /Cu(001) multilayer at a pressure of $<10^{-8}$ mbar at BESSY II. The sample is grown under ultrahigh vacuum conditions at a pressure $<10^{-9}$ mbar by molecular beam epitaxy. The materials are thermally evaporated by electron bombardment using a commercial evaporator onto a pristine Cu(001) single-crystal substrate cleaned by cycles of argon ion sputtering and annealing up to 800 K. Surface cleanliness and integrity are ensured by Auger electron spectroscopy and low-energy electron diffraction. Layer thicknesses are monitored during growth by medium-energy electron diffraction, allowing for precise thickness control down to single layers. Static characterization of the magnetization is performed after growth by measuring the longitudinal magneto-optical Kerr effect. The sample is field-cooled in a 60 mT external field from 400 K down to 120 K. The experiments are conducted at the slicing facility at BESSY II in Berlin, which offers x-ray pulses of 100 fs full-width half-maximum (FWHM) at variable photon energies over the $L_{2,3}$ resonances of the $3d$ metals investigated here, in combination with 800-nm laser pump pulses of 60 fs FWHM with variable fluence. The repetition rate of the x-ray pulses is 6 kHz and the one of the laser pump pulses 3 kHz, allowing to measure the sample with and without laser excitation in an alternating manner. The x-ray spot is about $140\ \mu\text{m} \times 120\ \mu\text{m}$ in size with a photon flux of around $10^6\ \text{photons s}^{-1}$ ($0.1\% \text{ bandwidth}^{-1}$). The photon energy resolution is around $E/\Delta E \simeq 250$. The laser fluence is calculated from the spot size, about $350 \times 550\ \mu\text{m}^2$, which is large enough to conveniently cover the x-ray spot, and from the average laser power of up to 1 W. A magnetic field of ± 300 mT is applied parallel to the sample surface in the plane of incidence. This is sufficient to reach magnetic saturation, as shown by field-dependent static x-ray magnetic circular dichroism measurements in reflectivity presented in Fig. 2. The magnetic circular dichroism is measured by reversing the direction of the field. The reflected x-ray intensity is recorded at a specific energy and angle for different pump-probe delay

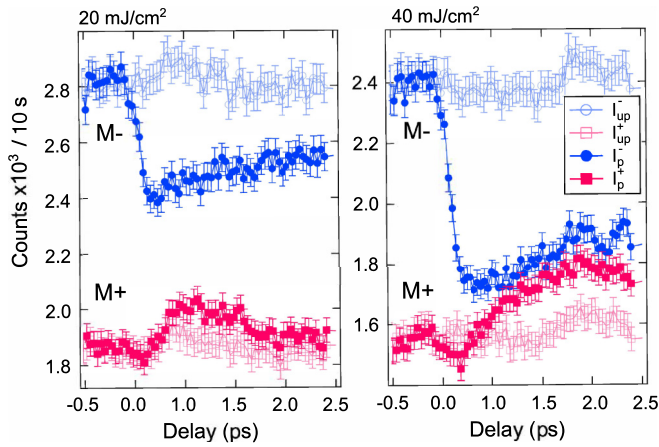


FIG. 3. Delay-time traces of reflected intensity, integrated for 10 s per data point, for circular polarization and opposite magnetization directions with two incident fluences, 20 and 40 mJ/cm². One measurement consists of four curves, pumped (solid symbols) and unpumped (open symbols) for both channels, $M+$ and $M-$. The experimental error is estimated by the total photon count N as \sqrt{N} .

times and pump fluences to study the response of the samples to the laser stimulus. Here, we focus only on the Co layer. The best measurement conditions, i.e., the parameter combination of angle and energy, are characterized by a figure of merit described by the product of reflected photon intensity and square of the static dichroic signal, which is inversely proportional to the necessary acquisition time. The maximum figure of merit was found at 7° between surface and beam and 778.1 eV photon energy, slightly on the falling edge of the Co L_3 resonance, with a maximum intensity of around 400 counts/s. All measurements were performed at a sample temperature of 390 K, above the Néel temperature of the Ni₃₁Mn₆₉ layer [33].

We aim to investigate to which extent the data can be quantitatively interpreted. We perform this analysis by looking at the difference and sum signals of the recorded delay time traces for the two magnetization directions. The difference signal is usually considered to be proportional to the magnetization, while a change of the sum signal has to be interpreted as a combination of electronic repopulation and structural dynamics that affects the optical response of the sample as illustrated in Fig. 1.

Typical pump-probe delay-time traces for Co are shown in Fig. 3 for two different incident laser fluences of 20 mJ/cm² and 40 mJ/cm². The time evolution after laser excitation is captured by recording the x-ray intensity for different delay times between pump and probe pulses. Each data point is acquired alternately, once without a laser pump and once with the laser pulse being present, in the following labeled as pumped (I_p) and unpumped (I_{up}), to rule out any kind of drift of the sample, x-ray beam, or laser while conducting the measurements. In total, for each pump-probe delay time, four signals are acquired, two for each direction of magnetization, I_p^+ , I_{up}^+ and I_p^- , I_{up}^- before moving to the next delay time. The recorded intensities after pumping in Fig. 3 are interpreted as illustrated in Fig. 1.

It is observed that the magnitude of change for each magnetization direction is not the same and, furthermore, that

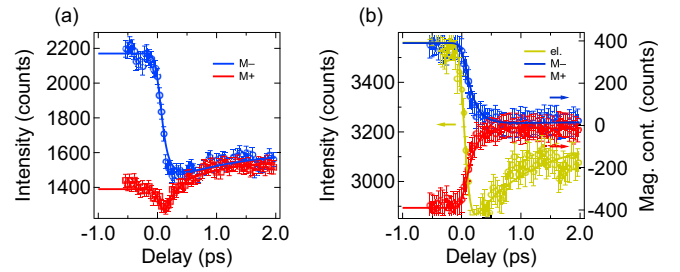


FIG. 4. Dynamic response of the signal at 50 mJ/cm² incident fluence. The separate symmetric and antisymmetric contributions, shown in (b), to the measured signal, presented in (a), are obtained from the sum and difference signals to the recorded traces as described in the text.

the higher pump fluence leads to an initial drop of intensity in both channels. This indicates two different timescales or at least magnitudes for changes in the total reflectivity and magnetic dichroism. In the time evolution of the $M-$ channel, no qualitative difference with higher fluence is observed, and the dynamics remain similar for the two fluences, only the magnitude increases. Since both channels evolve in the same direction initially at high fluence, the difference signal is slowed down relative to measurements at lower fluences.

The result from disentangling the experimental signals is shown in Fig. 4. The measured signals are reproduced by a superposition of a magnetic (antisymmetric) and a symmetric change of the intensity. The intensity $I(t)$ of each of the curves can be modeled by double-exponential functions of the form $I(t) = \pm C(\Theta(t_0)(A(\exp(-t/t_{de}) - 1) - B(\exp(-t/t_{re}) - 1) + 1))$ with the Heaviside function $\Theta(t_0)$, the amplitude of increase and decrease A and B , the initial intensity C , and the two time constants t_{de} and t_{re} of the dynamics. One such function is used to model the antisymmetric and one the symmetric dynamics. To model the antisymmetric dynamics, merely the sign of the signal change and the initial value are different for the curves corresponding to opposite magnetization. Fitting the 50-mJ/cm² data yields a time constant $t_{de}^{ele} = (100 \pm 30)$ fs for the symmetric change and $t_{de}^{mag} = (250 \pm 60)$ fs for the antisymmetric one. From comparison to theoretical simulations as shown below, we conclude that the symmetric change in reflectivity is mainly due to changes in the electronic system. The time constant of the recovery $t_{re}^{ele} = (1.0 \pm 0.2)$ ps of the electronic system is much faster than the magnetic one with $t_{re}^{mag} = (48 \pm 7)$ ps. We show that also in XRM, in the investigated case, the signal can be described in this fashion and that the combination of electronic and magnetic evolution allows a complete reconstruction of the observed signal and provides a comprehensive picture of the dynamics of each channel. This is not *a priori* the case since only a narrow reflection angle is probed, and the acquired signal, a combination of the transient change in refraction and absorption, results from the complete complex optical response in the acquisition energy window.

III. CALCULATIONS

The calculation of the angle-dependent reflected x-ray intensity in a multilayer system requires knowledge about the magneto-optical constants of the elements together with

TABLE I. Material constants used for the simulation of transient heat and strain in udkm1Dsim. The heat capacity is described by a linear approximation using a reduced temperature $T' = T/K$.

| Constants | NiMn | Co | Cu |
|--|---------------------|--------------------|---------------------|
| Vertical layer distance (Å) | 1.71 [36] | 1.74 [37] | 1.81 [38] |
| Sound velocity (nm/ps) | 5.150 [39] | 4.270 [39] | 3.570 [40] |
| Lin. thermal expansion ($10^{-6}/K$) | 15 [41] | 12 [42] | 17 [42] |
| Thermal conductivity [W/(m K)] | 7.8 [43] | 90 [43,44] | 361 [44] |
| Heat capacity [J/(kg K)] | $495 + 0.28T'$ [45] | $693 + 0.6T'$ [45] | $350 + 0.11T'$ [45] |

precise information about their spatial arrangement. A general description of the approach can be found in Ref. [17], for example. We use static absorption spectra to find the magneto-optical constants in equilibrium, while the sample structure is defined by monitoring the thickness during growth as described before. The full refractive index is defined here as

$$n = 1 - (\delta + \Delta\delta) + i(\beta + \Delta\beta) \quad (1)$$

with the magnetic contributions $\Delta\delta$ and $\Delta\beta$.

In order to reproduce the time-dependent signals measured in the experiment and to relate them to transient magnetization, strain, and electronic occupation, we use two different approaches. In the first, we use a purely thermal model, in which we consider laser-induced heat and strain and calculate the static optical response. In this treatment, the heat introduced by the laser excitation reduces the macroscopic magnetization. Furthermore, the lattice expands or compresses due to coherent phonon excitation, leading to transient strain profiles. A strained lattice influences the XRMR due to the new transient geometry. No change of the elemental magneto-optical response due to the electronic transitions excited by the laser pulse is considered in this approach. The magneto-optical constants are derived from static absorption spectra recorded in total electron yield. From the absorption, $\beta + \Delta\beta$, the imaginary part of the refractive index, is obtained. The real part is then calculated by a Kramers-Kronig transform. For this to work well, information over a larger energy range is necessary. The values for β for off-resonant energies are taken from literature [34] and are replaced with the measured absorption curves in the recorded energy range around the $L_{2,3}$ resonances. The magnetic contribution is found by evaluating the difference of the real and imaginary parts for the two opposite magnetization directions recorded.

The simulation of the reflected intensities for the investigated angle of 7° between the sample surface and beam is then performed using the udkm1Dsim script developed in the group of M. Bargheer by D. Schick *et al.* [35]. The sample is treated as a 110 Å Cu/25 Å Co/31 Å Mn/Cu(100), as measured in the sample characterization. Magnetization is modeled by a critical exponent law and is described by $M(t) \propto (1 - T/T_c)^{3/2}$ with a reduced $T_c = 1300$ K for Co due to the thin layer. Time-dependent reflectivity is obtained after instantaneous excitation by a 60 fs FWHM laser pulse with a fluence of 80 mJ/cm² centered at a wavelength of 800 nm. The absorbed laser power is calculated considering multilayer absorption and reflection, giving rise to an elevated temperature $T(t)$. The temperature profile for each delay time is obtained by evaluating the heat diffusion after the initial

excitation on a discrete temporal and spatial grid. The temporal evolution is calculated in 50 fs steps and spatially the grid is interpolated to 11 points for each atomic distance to avoid large gradients. The material parameters employed in the calculation are listed in Table I. For Ni_{0.31}Mn_{0.69}, the literature values of Mn are used since no values for the alloy are available. The reflected intensity is convoluted with a Gaussian of 3.2 eV FWHM, mimicking the experimental resolution, and the temporal evolution by a Gaussian of 100 fs FWHM, representing the width of the experimental probe pulse. The transient strain on the lattice is included in the simulation and leads to deviations from the simple exponential ultrafast change of the integrated reflected intensity at early timescales.

In the second approach, we investigate the excited correlated electronic and magnetic densities in terms of the time-dependent optical response function. The dynamic optical response is calculated by time-dependent density-functional theory (TD-DFT). The transient response function of Co is evaluated after excitation with an ultrashort laser pulse of 60 fs FWHM and 23 mJ/cm² incident fluence to judge the influence of the electronic system on the observables. The calculations are based on a noncollinear version of the Elk code [46], where electron dynamics after laser excitation is treated by taking into account relativistic effects. A comparison of the optical response function obtained in the static experiment and the calculated transient response function at different delay times is presented in Fig. 5. The zero of the delay time for the simulations is defined at the center of the exciting pulse. At the peak maxima of the absorption, both the real and the imaginary part of the refractive index reduce on an ultrafast timescale as a result of the excitation. Electronic repopulation is recognized from the increase in β in the rising flank of the Co absorption peaks, at around 775 and 791 eV. The demagnetization manifests itself as a reduction of $\Delta\beta$ at both the L_3 and L_2 edges.

The TD-DFT-calculated transient response function is included in quasistatic calculations of the reflected intensity at 7° using ReMagX [20,47]. The layer structure is the same as in the first approach. The reflected intensity is calculated using the matrix formalism. For Cu and Ni₃₁Mn₆₉, tabulated values of the optical constants from [48] are employed. The resulting spectra of the reflected intensity are convoluted by a Gaussian with 3.2 eV FWHM.

IV. RESULTS AND DISCUSSION

Figure 6 shows in panel (a) the experimental reflectivity spectra of the Co L_3 edge at negative time delays, i.e., the

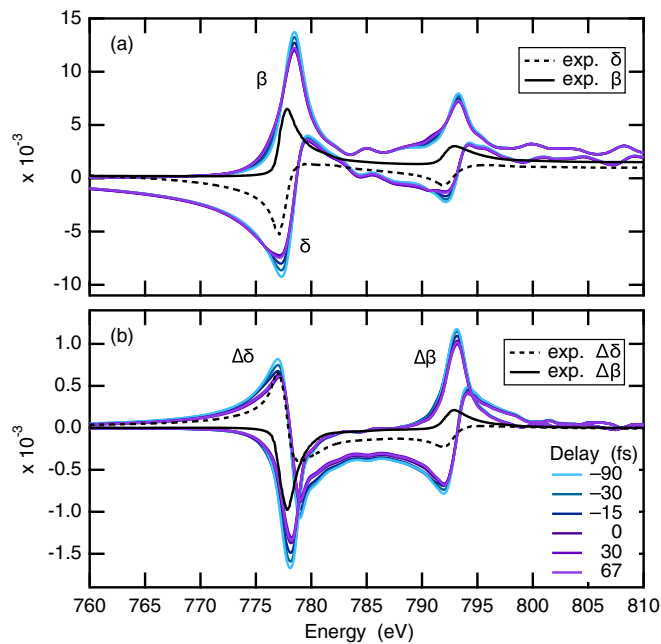


FIG. 5. Comparison of time-dependent magneto-optical parameters after laser excitation in Co obtained by TD-DFT to the static ones obtained from experimental data. (a) Nonmagnetic part of the refractive index, δ and β , calculated at different times after excitation by a 60-fs laser pulse, centered at delay time zero. (b) Calculated magnetic contributions to the refractive index. The dashed and solid black lines denote the optical response extracted from static measurements of the absorption.

static spectra, for the two magnetization directions. Panels (b) and (c) present the results of the two simulation approaches for three different delay times each. Panel (b) shows the calculated transient signal acquired with the first approach, the thermal model, while panel (c) presents the results obtained from the time-dependent optical response function. The magnetic circular dichroism is recognized from the difference between the $M+$ and the $M-$ channels. While in the thermal approach [Fig. 6(b)], the intensity of the $M+$ channel at the L_3 edge increases with delay time after the pump pulse, both channels decrease in intensity in the electronic-structure approach [Fig. 6(c)].

To benchmark to which extent the XRMR results resemble an absorption measurement, we perform simulations of the reflectivity using truncated optical response functions in which either the real or the imaginary part is set to zero. Comparing the results with the simulation of the reflectivity employing the full response function then allows estimating the influence of each part. The result of this estimation for an angle of 7° is presented in Fig. 7. At this angle, the reflected intensity at the Co L_3 edge cannot be ascribed to a single part of the refractive index. While in the rising flank of the L_3 peak the reflected intensity is dominated by the contribution from the real part of the refractive index, at the probed energy of 778.1 eV, both the imaginary part, linked to the energy-loss mechanisms and thus the absorptive part of the interaction, and the real part, i.e., the reflective part, contribute.

The comparison of the normalized experimental sum and difference signals as a function of delay time with the two

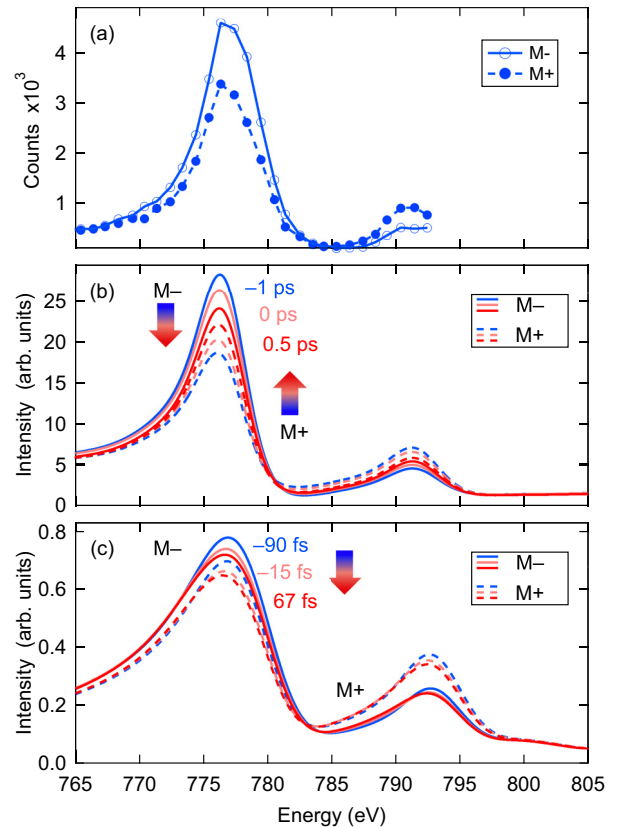


FIG. 6. Comparison of experimentally recorded reflected intensity at 7° over the Co L_3 resonance with calculated transient spectra. Curves corresponding to the different magnetization directions are denoted as solid ($M-$) and dashed ($M+$) lines. (a) Recorded spectrum at negative delay times. (b) Calculated reflectivity at different delay times up to 0.5 ps after laser excitation. The calculation assumes a heat-induced quench of the magnetization and lattice compression. (c) Simulated reflected intensity at 7° using the transient magneto-optical function obtained by TD-DFT. The signals for both magnetization directions decrease within 67 fs at the peak maxima.

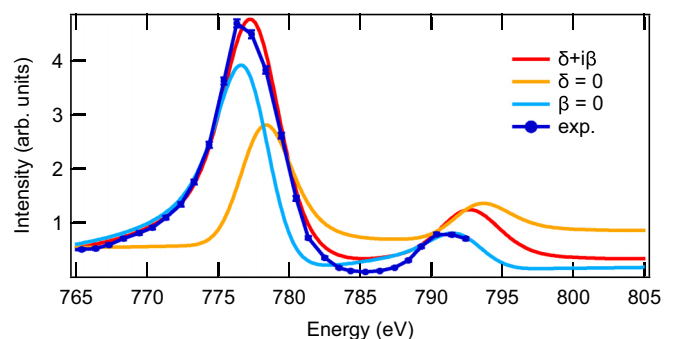


FIG. 7. Simulated reflected intensity at 7° using the full refractive index (red), only the real part of the refractive index (blue), and only the imaginary part (orange). At the probed energy of 778.1 eV, the experimental intensity is neither described considering only the real or only the imaginary part of the refractive index. Considering the experimental resolution of around 3 eV, the recorded trace can thus not be straightforwardly interpreted in the same fashion as an absorption spectrum.

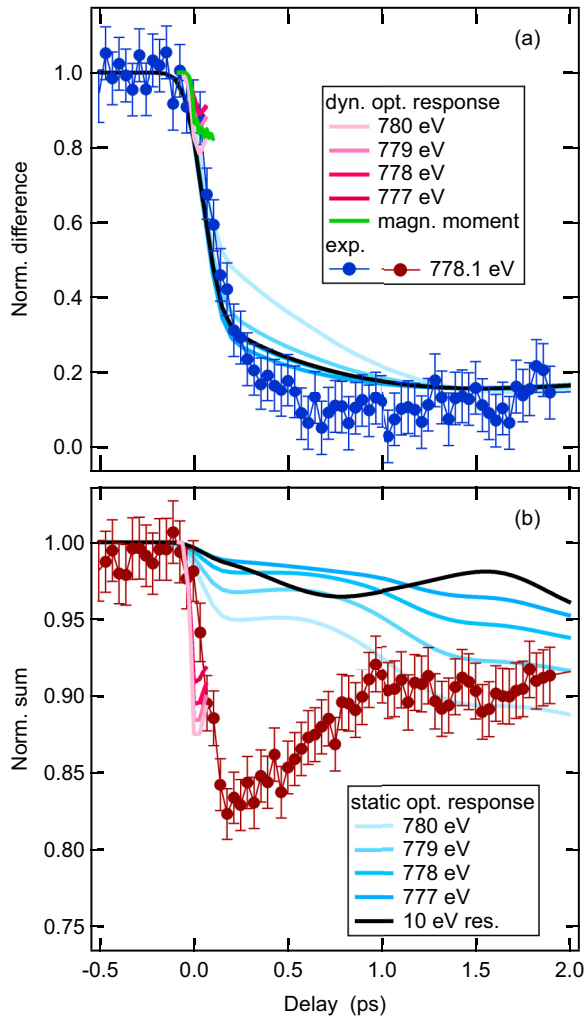


FIG. 8. Comparison of the calculated changes of the difference and sum signals after laser excitation to experimental data (filled symbols) at 40 mJ/cm^2 incident fluence. (a) Difference, (b) sum of the reflectivities for the two magnetization directions, compared to results of the calculations performed with static magneto-optical functions in a thermal model (bluish lines) and with dynamic ones from TD-DFT (reddish lines). Simulation results employing different center positions of the 3.2 eV FWHM Gaussian window of energy convolution are shown, as indicated in the legend, mimicking measurements at different photon energies. The TD-DFT-calculated total magnetic moment is presented by a green line in (a). Lastly, the simulated traces of the thermal model using a very large energy window of 10 eV FWHM (black lines) are plotted to simulate a measurement that integrates over the whole absorption edge.

simulation approaches is presented in Fig. 8. To assess the influence of the photon energy, the temporal behavior of the simulated reflectivities has been evaluated at different photon energies for each of the approaches, as denoted in the legend. In the simulation approach in which the transient thermal changes of the sample are considered (bluish lines in Fig. 8), the ultrafast drop in the difference signal and thus the magnetization are reproduced well, presented in Fig. 8 in the top panel. The heat stimulus by the fs laser pulse quenches the magnetization and, consequently, the dichroic difference

reduces within 0.5 ps . The thermal simulations do not describe the experimentally recorded sum signal, though, as shown in the bottom panel of Fig. 8, since the fast drop of the sum signal is not captured. While the experiment shows a sudden drop in the reflectivity, the simulated sum signal in this approach stays almost constant even in the presence of temperature-induced strain and reduces only slowly on a longer timescale.

In the second approach, in which the simulation is realized by calculating the reflectivity from time-dependent response functions obtained by TD-DFT, the ultrafast quench of the difference signal is also reproduced. Since these calculations do not include any spin flips at scattering centers caused by crystalline imperfections nor magnon-induced demagnetization mechanisms, the amplitude of demagnetization is smaller than in the experiment and also stops at earlier times after the excitation. Contrary to the first approach when considering only a heat pulse, the simulations employing the transient optical response do well reproduce the ultrafast drop of the reflectivity recorded in the experiment [Fig. 8(b)]. Qualitatively, they also show the faster change of the sum signal, which reaches its plateau after about 90 fs , compared to the difference signal, which reaches its minimum after 120 fs .

The comparison of the presented calculations to the experimental data now allows us to draw conclusions about the nature of the ultrafast drop of the helicity-averaged reflectivity. Since it is reproduced only when electronic effects are included in the simulations, we can conclude that the fast reduction of the reflectivity must be due to transient repopulations of the electronic system. Ultrafast lattice contraction (or expansion) driven by laser heating, which in principle can also lead to a sudden decrease (or increase) of the intensity measured under a certain angle [23], does obviously not play a role here at short times. Intrinsically, the phononic influence lives on longer timescales than the light-induced electronic changes, and may play a significant role at longer times, as the bluish lines in Fig. 8(b) indicate. Since the experimental dynamics are longer in time than what can be reasonably accessed in TD-DFT, a definite description of the driving mechanism can only be acquired in time-resolved recordings over the full spectral range of the Co $L_{2,3}$ edge.

The ultrafast drop of the magnetic signal of the Co layer can be compared to previous results from literature. Gdde *et al.* observed for an about 70% demagnetization a time constant faster than their pulse width of 150 fs in a 3-ML Co film on Cu(001), using second-harmonic generation [29]. In contrast to our result, they could not observe different time constants for the sum and the difference signals, i.e., for the electronic and magnetic contribution. Cinchetti *et al.* compared time-resolved magneto-optical Kerr effect of 10-nm Co/Cu(001) to time-resolved two-photon photoemission and found, in contrast to Ref. [29] and in agreement with our result, that the electronic excitation, detected by two-photon photoemission, occurs on shorter timescales than the demagnetization, observed by time-resolved magneto-optical Kerr effect [30]. The latter showed a maximum demagnetization at about 400 fs for 15% demagnetization, and around 750 fs for a demagnetization of approximately 50% [30]. The shift of the time of maximum demagnetization to larger values with higher pump fluence has been interpreted by assuming Elliott-Yafet-type spin-flip scattering of electrons with impurities or

phonons [30]. The demagnetization time found in Ref. [30] for the larger fluence agrees with our result shown in Fig. 8(a), where for 90% demagnetization the minimum of the curve is reached after about 700 fs.

Chen *et al.* have studied the transfer of optically excited electronic spin currents between Co and Cu in 3 and 5 ML Co/Cu(001) by time-resolved second-harmonic generation [31]. In agreement with our results, the sum signal representing the electronic response exhibits a faster reaction on the excitation, on the timescale of the temporal resolution of the experiment, and also a faster recovery than the magnetic difference signal [31].

For the NiMn composition of Ni₃₁Mn₆₉ and the thickness of 20 ML, the antiferromagnetic ordering temperature of NiMn can be estimated to about 360 K [33,36,49]. Above its ordering temperature, the NiMn layer does not influence the Co layer magnetically [36], but the presence of the additional layer and of exchange-coupled magnetic moments at the interface to the Co layer may be influential via transient nonlocal effects such as the interchange or the reflection of electronic spin currents at the Co/NiMn interface [15]. However, from the comparison to the existing results on Co/Cu(001) from literature mentioned above, a significant role of the additional interface between Co and the magnetically disordered NiMn layer for the ultrafast dynamics of the Co layer can not be discerned.

Assigning the symmetric change in reflected intensity to electronic contributions and the antisymmetric one to magnetic, the information obtained from the analysis of the two channels in a time-resolved soft-x-ray XRM R experiment is equivalent to that of other time-resolved techniques, but offers the additional advantage of being element-selective in a straightforward way. In addition, the depth sensitivity of XRM R, which allows the analysis in terms of a magnetic depth profile [17–21], may be applied also to time-resolved measurements. Qualitative depth information has already been achieved in time-resolved magneto-optical Kerr-effect measurements by exploiting the different probing depths of Kerr rotation and ellipticity and has helped to disentangle the timescales of the effects of nonlocal spin transport and local spin-flip scattering of thermalized electrons in Co/Cu(001) [32]. However, because of the large wavelength of visible light and the short penetration depth, this works well only for a limited number of layers and relatively thick layers, while in XRM S using soft x rays, quantitative depth information can be obtained even on a nanometer scale by tuning the reflection angle and the probe photon energy [17–21].

The influence of a finite probing-energy window in the experiment is investigated by calculating the time evolution at different energies over the resonance. It reveals a dependence of both, the fast quench of circular dichroism and the reduction of the sum signal on the photon energy in both simulation approaches. It has thus to be kept in mind when interpreting experimental data. However, the general trend and qualitative outcome do not depend on the photon energy at which the temporal behavior is studied. The black lines in Fig. 8 are the result of averaging the thermal simulation over an energy range of 10 eV, which includes the entire Co L_3 edge. They qualitatively match with the other results of the same simulation. The green line in Fig. 8(a) is the transient

total magnetic moment as obtained from the TD-DFT calculations. The simulations yield the same fast decay of the difference signal at the different energies; however, there is not an exact proportionality between the simulated difference signal and the magnetic moment. Nonmagnetic electronic effects have thus also a certain influence on the difference signal. Overall, however, the assignment of the difference signal to the magnetic contribution is justified, while the sum signal for delay times up to 1 ps has to be attributed to nonmagnetic electronic excitations. We can assign these to the influence of the absorptive part of the optical properties on the reflectivity, in particular, to the variations of the calculated time-dependent β around the L_2 and L_3 absorption edges as seen in Fig. 5: After the excitation, previously occupied states become available for transitions, resulting in a higher absorption in the low-energy flank of the absorption peaks, while formerly unoccupied states are blocked by excited electrons, leading to a reduction in absorption at around the peak maxima.

The dependence of the amplitude of the difference signal on the probing energy is opposite for the two simulation approaches [Fig. 8(a)]. The decreasing demagnetization amplitude in the thermal model for higher energies may be explained with the mixing of signals from the L_3 and L_2 edges. At higher probing energies, an increasing amount of signal from the L_2 edge is measured, and since the magnetic circular dichroism reverses sign on the edges, the low energy resolution leads to a different observed demagnetization amplitude. Additionally, employing a 10-eV energy resolution and thereby integrating over the full L_3 resonance in the simulation, does not result in significantly different demagnetization dynamics. In conclusion, the simulations show only a minor sensitivity of the observable in XRM R to the probing energy. This is particularly helpful when comparing different measurements with different energy resolutions.

A shift and small decrease of the x-ray resonance has been calculated [50] and reported for Ni in absorption measurements [7,27,51] and has also been found in investigations of transition-metal $M_{2,3}$ edges [28]. A strong decrease of the reflected intensity has not yet been reported, but measurements of time-resolved Co reflectivity spectra over the entire L_3 resonance are still missing and could clarify which of the processes dominate in the experiment. Results obtained in absorption on Co are reported in a preprint [52], indicating a small decrease together with a slight shift of the Co L_3 absorption peak.

Electronic changes could be phenomenologically implemented in the thermal simulations by assuming an *ad hoc* energy shift of up to 300 meV, with a temporal profile of the shift taken from the temporal intensity profile of the experimental sum signal. This results in an excellent agreement between the heat-diffusion simulations and the experiment. Similarly, the data can also be reproduced by assuming an overall reduction of the resonance peak.

V. SUMMARY AND CONCLUSIONS

The presented work provides insight into the interpretation of time-resolved x-ray circular dichroism data in reflectivity,

which is widely employed to study ultrafast processes in an element- and time-resolved fashion. The temporal behavior of the two channels recorded in the experiment is explained in terms of a combination of a symmetric decrease of the reflected intensities together with a convergence of the signals due to a quench of the magnetization, as presented in Fig. 4. The experimental results are simulated by a heat-diffusion model and by a nonequilibrium electron density calculation to investigate the origin of the different electronic and magnetic dynamics. Three factors are identified that promote a symmetric change of the XRM channels as observed in the experiment—a shift of the resonance, an overall reduction of the reflectivity due to electron-state filling, and, on the longer timescale, a reduction of the reflectivity due to heat-induced lattice strain. The latter alone does not explain the observed ultrafast reduction of the reflected intensity.

A certain probing-energy dependence of the observed evolution of the magnetic signal is supported by calculations of the delay-time-dependent magneto-optical constants and simulations of the XRM at different probing energies. We

show that the effect is negligible on the resonance edge even with a small finite-energy window of about 3 eV, as long as the resonance edges are well separated.

In conclusion, this allows us to finally state that even with a limited energy window, qualitative information about the transient magnetic state of the system is obtained in XRM. With the help of simulations, it will be possible to take advantage of the full power of XRM to study the interplay between magnetization dynamics and the structural and electronic properties on ultrafast timescales in an element-resolved manner.

ACKNOWLEDGMENTS

This work was supported by the Deutsche Forschungsgemeinschaft (DFG, German Research Foundation) Project-ID 328545488 CRC/TRR 227 “Ultrafast Spin Dynamics” (Projects A02, A03, A04, and A07). We thank the Helmholtz-Zentrum Berlin for the allocation of synchrotron radiation beamtime.

-
- [1] E. Beaurepaire, J.-C. Merle, A. Daunois, and J.-Y. Bigot, Ultrafast Spin Dynamics in Ferromagnetic Nickel, *Phys. Rev. Lett.* **76**, 4250 (1996).
- [2] A. Kirilyuk, A. V. Kimel, and T. Rasing, Ultrafast optical manipulation of magnetic order, *Rev. Mod. Phys.* **82**, 2731 (2010).
- [3] J. Walowski and M. Münzenberg, Perspective: Ultrafast magnetism and THz spintronics, *J. Appl. Phys.* **120**, 140901 (2016).
- [4] M. Fähnle, M. Haag, C. Illg, B. Mueller, W. Weng, T. Tsatsoulis, H. Huang, J. Briones, N. Teeny, L. Zhang, and T. Kuhn, Review of ultrafast demagnetization after femtosecond laser pulses: A complex interaction of light with quantum matter, *Am. J. Mod. Phys.* **7**, 68 (2018).
- [5] P. Scheid, Q. Remy, S. Lebègue, G. Malinowski, and S. Mangin, Light induced ultrafast magnetization dynamics in metallic compounds, *J. Magn. Magn. Mater.* **560**, 169596 (2022).
- [6] B. Koopmans, G. Malinowski, F. Dalla Longa, D. Steiauf, M. Fähnle, T. Roth, M. Cinchetti, and M. Aeschlimann, Explaining the paradoxical diversity of ultrafast laser-induced demagnetization, *Nat. Mater.* **9**, 259 (2010).
- [7] C. Stamm, T. Kachel, N. Pontius, R. Mitzner, T. Quast, K. Holldack, S. Khan, C. Lupulescu, E. F. Aziz, M. Wietstruk, H. A. Dürr, and W. Eberhardt, Femtosecond modification of electron localization and transfer of angular momentum in nickel, *Nat. Mater.* **6**, 740 (2007).
- [8] C. Boeglin, E. Beaurepaire, V. Halté, V. López-Flores, C. Stamm, N. Pontius, H. A. Dürr, and J.-Y. Bigot, Distinguishing the ultrafast dynamics of spin and orbital moments in solids, *Nature (London)* **465**, 458 (2010).
- [9] M. Wietstruk, A. Melnikov, C. Stamm, T. Kachel, N. Pontius, M. Sultan, C. Gahl, M. Weinelt, H. A. Dürr, and U. Bovensiepen, Hot-Electron-Driven Enhancement of Spin-Lattice Coupling in Gd and Tb 4*f* Ferromagnets Observed by Femtosecond X-Ray Magnetic Circular Dichroism, *Phys. Rev. Lett.* **106**, 127401 (2011).
- [10] I. Radu, K. Vahaplar, C. Stamm, T. Kachel, N. Pontius, H. A. Dürr, T. A. Ostler, J. Barker, R. F. L. Evans, R. W. Chantrell *et al.*, Transient ferromagnetic-like state mediating ultrafast reversal of antiferromagnetically coupled spins, *Nature (London)* **472**, 205 (2011).
- [11] D. Rudolf, C. La-O-Vorakiat, M. Battiato, R. Adam, J. M. Shaw, E. Turgut, P. Maldonado, S. Mathias, P. Grychtol, H. T. Nembach *et al.*, Ultrafast magnetization enhancement in metallic multilayers driven by superdiffusive spin current, *Nat. Commun.* **3**, 1037 (2012).
- [12] A. Eschenlohr, M. Battiato, P. Maldonado, N. Pontius, T. Kachel, K. Holldack, R. Mitzner, A. Föhlisch, P. M. Oppeneer, and C. Stamm, Ultrafast spin transport as key to femtosecond demagnetization, *Nat. Mater.* **12**, 332 (2013).
- [13] N. Berggaard, V. López-Flores, V. Halté, M. Hehn, C. Stamm, N. Pontius, E. Beaurepaire, and C. Boeglin, Ultrafast angular momentum transfer in multisublattice ferrimagnets, *Nat. Commun.* **5**, 3466 (2014).
- [14] E. Turgut, D. Zusin, D. Legut, K. Carva, R. Knut, J. M. Shaw, C. Chen, Z. Tao, H. T. Nembach, T. J. Silva, S. Mathias, M. Aeschlimann, P. M. Oppeneer, H. C. Kapteyn, M. M. Murnane, and P. Grychtol, Stoner versus Heisenberg: Ultrafast exchange reduction and magnon generation during laser-induced demagnetization, *Phys. Rev. B* **94**, 220408(R) (2016).
- [15] I. Kumberg, E. Goliaş, N. Pontius, R. Hosseinifar, K. Frischmuth, I. Gelen, T. Shinwari, S. Thakur, C. Schüßler-Langeheine, P. M. Oppeneer, and W. Kuch, Accelerating the laser-induced demagnetization of a ferromagnetic film by antiferromagnetic order in an adjacent layer, *Phys. Rev. B* **102**, 214418 (2020).
- [16] E. Goliaş, I. Kumberg, I. Gelen, S. Thakur, J. Gördes, R. Hosseinifar, Q. Guillet, J. Dewhurst, S. Sharma, C. Schüßler-Langeheine, N. Pontius, and W. Kuch, Ultrafast Optically Induced Ferromagnetic State in an Elemental Antiferromagnet, *Phys. Rev. Lett.* **126**, 107202 (2021).
- [17] M. Elzo, E. Jal, O. Bunau, S. Grenier, Y. Joly, A. Ramos, H. Tolentino, J. Tonnerre, and N. Jaouen, X-ray resonant magnetic reflectivity of stratified magnetic structures: Eigenwave formalism and application to a W/Fe/W trilayer, *J. Magn. Magn. Mater.* **324**, 105 (2012).

- [18] J.-M. Tonnerre, M. Przybylski, M. Ragheb, F. Yildiz, H. C. N. Tolentino, L. Ortega, and J. Kirschner, Direct in-depth determination of a complex magnetic configuration in an exchange-coupled bilayer with perpendicular and in-plane anisotropy, *Phys. Rev. B* **84**, 100407(R) (2011).
- [19] J. B. Kortright, Resonant soft x-ray and extreme ultraviolet magnetic scattering in nanostructured magnetic materials: Fundamentals and directions, *J. Electron Spectrosc. Relat. Phenom.* **189**, 178 (2013).
- [20] S. Macke and E. Goering, Magnetic reflectometry of heterostructures, *J. Phys.: Condens. Matter* **26**, 363201 (2014).
- [21] E. Jal, M. Dąbrowski, J.-M. Tonnerre, M. Przybylski, S. Grenier, N. Jaouen, and J. Kirschner, Magnetization profile across Au-covered bcc Fe films grown on a vicinal surface of Ag(001) as seen by x-ray resonant magnetic reflectivity, *Phys. Rev. B* **87**, 224418 (2013).
- [22] E. Jal, M. Dąbrowski, J. M. Tonnerre, M. Przybylski, S. Grenier, N. Jaouen, and J. Kirschner, Noncollinearity of the canted spins across ultrathin Fe films on vicinal Ag surfaces, *Phys. Rev. B* **91**, 214418 (2015).
- [23] E. Jal, V. López-Flores, N. Pontius, T. Ferté, N. Berggaard, C. Boeglin, B. Vodungbo, J. Lüning, and N. Jaouen, Structural dynamics during laser-induced ultrafast demagnetization, *Phys. Rev. B* **95**, 184422 (2017).
- [24] N. Thielemann-Kühn, D. Schick, N. Pontius, C. Trabant, R. Mitzner, K. Hollmack, H. Zabel, A. Föhlich, and C. Schüßler-Langeheine, Ultrafast and Energy-Efficient Quenching of Spin Order: Antiferromagnetism Beats Ferromagnetism, *Phys. Rev. Lett.* **119**, 197202 (2017).
- [25] V. Chardonnet, M. Hennes, R. Jarrier, R. Delaunay, N. Jaouen, M. Kuhlmann, N. Ekanayake, C. Léveillé, C. von Korff Schmising, D. Schick, K. Yao, X. Liu, G. S. Chiuzbăian, J. Lüning, B. Vodungbo, and E. Jal, Toward ultrafast magnetic depth profiling using time-resolved x-ray resonant magnetic reflectivity, *Struct. Dyn.* **8**, 034305 (2021).
- [26] C. T. Chen, Y. U. Idzerda, H.-J. Lin, N. V. Smith, G. Meigs, E. Chaban, G. H. Ho, E. Pellegrin, and F. Sette, Experimental Confirmation of the X-Ray Magnetic Circular Dichroism Sum Rules for Iron and Cobalt, *Phys. Rev. Lett.* **75**, 152 (1995).
- [27] T. Kachel, N. Pontius, C. Stamm, M. Wietstruk, E. F. Aziz, H. A. Dürr, W. Eberhardt, and F. M. F. de Groot, Transient electronic and magnetic structures of nickel heated by ultrafast laser pulses, *Phys. Rev. B* **80**, 092404 (2009).
- [28] K. Yao, F. Willems, C. von Korff Schmising, I. Radu, C. Strüber, D. Schick, D. Engel, A. Tsukamoto, J. K. Dewhurst, S. Sharma, and S. Eisebitt, Distinct spectral response in M-edge magnetic circular dichroism, *Phys. Rev. B* **102**, 100405(R) (2020).
- [29] J. Güdde, U. Conrad, V. Jähnke, J. Hohlfeld, and E. Matthias, Magnetization dynamics of Ni and Co films on Cu(001) and of bulk nickel surfaces, *Phys. Rev. B* **59**, R6608 (1999).
- [30] M. Cinchetti, M. Sánchez Albaneda, D. Hoffmann, T. Roth, J.-P. Wüstenberg, M. Krauß, O. Andreyev, H. C. Schneider, M. Bauer, and M. Aeschlimann, Spin-Flip Processes and Ultrafast Magnetization Dynamics in Co: Unifying the Microscopic and Macroscopic View of Femtosecond Magnetism, *Phys. Rev. Lett.* **97**, 177201 (2006).
- [31] J. Chen, U. Bovensiepen, A. Eschenlohr, T. Müller, P. Elliott, E. K. U. Gross, J. K. Dewhurst, and S. Sharma, Competing Spin Transfer and Dissipation at Co/Cu(001) Interfaces on Femtosecond Timescales, *Phys. Rev. Lett.* **122**, 067202 (2019).
- [32] J. Wieczorek, A. Eschenlohr, B. Weidtmann, M. Rösner, N. Berggaard, A. Tarasevitch, T. O. Wehling, and U. Bovensiepen, Competing spin transfer and dissipation at Co/Cu(001) interfaces on femtosecond timescales, *Phys. Rev. B* **92**, 174410 (2015).
- [33] T. Hagelschuer, Y. A. Shokr, and W. Kuch, Spin-state transition in antiferromagnetic Ni_{0.4}Mn_{0.6} films in Ni/NiMn/Ni trilayers on Cu(001), *Phys. Rev. B* **93**, 054428 (2016).
- [34] C. T. Chantler, Theoretical form factor, attenuation, and scattering tabulation for $Z = 1-92$ from $E = 1-10$ eV to $E = 0.4-1.0$ MeV, *J. Phys. Chem. Ref. Data* **24**, 71 (1995).
- [35] D. Schick, A. Bojahr, M. Herzog, R. Shayduk, C. von Korff Schmising, and M. Bargheer, UDKM1DSIM—A simulation toolkit for 1D ultrafast dynamics in condensed matter, *Comput. Phys. Commun.* **185**, 651 (2014).
- [36] C. Tieg, W. Kuch, S. G. Wang, and J. Kirschner, Growth, structure, and magnetism of single-crystalline Ni_xMn_{100-x} films and NiMn/Co bilayers on Cu(001), *Phys. Rev. B* **74**, 094420 (2006).
- [37] J. R. Cerda, P. L. de Andres, A. Cebollada, R. Miranda, E. Navas, P. Schuster, C. M. Schneider, and J. Kirschner, Epitaxial growth of cobalt films on Cu(100): A crystallographic LEED determination, *J. Phys.: Condens. Matter* **5**, 2055 (1993).
- [38] M. E. Straumanis and L. S. Yu, Lattice parameters, densities, expansion coefficients and perfection of structure of Cu and of Cu-In α phase, *Acta Crystallogr. Sect. A* **25**, 676 (1969).
- [39] G. V. Samsonov, *Handbook of the Physicochemical Properties of the Elements*, edited by G. V. Samsonov (Springer US, Boston, MA, 1968).
- [40] W. M. Haynes, D. R. Lide, and T. J. Bruno, *CRC Handbook of Chemistry and Physics*, 95th ed. (CRC Press, Boca Raton, FL, 2014).
- [41] K. Thurnay, *Thermal properties of transition metals*, *Tech. Rep. FZKA-6095* (Karlsruhe, Germany, 1998).
- [42] B. D. Dunn, *Materials and Processes* (Springer International Publishing, New York, 2016).
- [43] Z. Tong, S. Li, X. Ruan, and H. Bao, Comprehensive first-principles analysis of phonon thermal conductivity and electron-phonon coupling in different metals, *Phys. Rev. B* **100**, 144306 (2019).
- [44] J. Carvill, Thermodynamics and heat transfer, *Mechanical Engineer's Data Handbook* (Elsevier, Amsterdam, 1993).
- [45] M. W. Chase, C. A. Davies, J. R. Downey, Jr., D. J. Frurip, R. A. McDonald, and A. N. Syverud, JANAF Thermochemical Tables (3rd ed.), *J. Phys. Chem. Ref. Data* **14**, Suppl. 1 (1985).
- [46] J. Dewhurst, K. Krieger, S. Sharma, and E. Gross, An efficient algorithm for time propagation as applied to linearized augmented plane wave method, *Comput. Phys. Commun.* **209**, 92 (2016).
- [47] <https://www.remagx.org/>.
- [48] B. Henke, E. Gullikson, and J. Davis, X-ray interactions: Photoabsorption, scattering, transmission, and reflection at $E = 50-30000$ eV, $Z = 1-92$, *At. Data Nucl. Data Tables* **54**, 181 (1993).
- [49] M. Reinhardt, J. Seifert, M. Busch, and H. Winter, Magnetic interface coupling between ultrathin Co and Ni_xMn_{100-x} films on Cu(001), *Phys. Rev. B* **81**, 134433 (2010).

- [50] K. Carva, D. Legut, and P. M. Oppeneer, Influence of laser-excited electron distributions on the x-ray magnetic circular dichroism spectra: Implications for femtosecond demagnetization in Ni, *Europhys. Lett.* **86**, 57002 (2009).
- [51] C. Stamm, N. Pontius, T. Kachel, M. Wietstruk, and H. A. Dürr, Femtosecond x-ray absorption spectroscopy of spin and orbital angular momentum in photoexcited Ni films during ultrafast demagnetization, *Phys. Rev. B* **81**, 104425 (2010).
- [52] N. Pontius, J. K. Dewhurst, C. Schüssler-Langeheine, S. Jana, C. von Korff Schmising, S. Eisebitt, S. Shallcross, and S. Sharma, Mapping the energy-time landscape of spins with helical x-rays, [arXiv:2205.03172](https://arxiv.org/abs/2205.03172).